Characterization and Optimization of Highly Efficient Silicon-Based Textured Solar Cells: Theory and Experiment

A.V. Sachenko[1], V.P. Kostylyov[1], V.M. Vlasiuk[1], I.O. Sokolovskyi[1], M. Evstigneev[2], A.I. Shkrebtii[3*], D. Johnston[4], P. Michael[4], and T. Missimer[4]

[1] V. Lashkaryov Institute of Semiconductor Physics, NAS of Ukraine, 03028 Kyiv, Ukraine
[2] Department of Physics and Physical Oceanography, Memorial University of Newfoundland, St. John's, NL, A1B 3X7, Canada
[3] Ontario Tech University, Oshawa, ON, L1G 0C5, Canada
[4] Florida Gulf Coast University, Fort Myers, Florida 33913, USA
[*]Corresponding author: Anatoli.Chkrebtii@ontariotechu.ca

2021 IEEE 48th Photovoltaic Specialists Conference (PVSC) | 978-1-6654-1922-2/21/$31.00 ©2021 IEEE | DOI: 10.1109/PVSC43889.2021.9518764

***Abstract*—We developed and applied an improved theoretical model to optimize characteristics of highly efficient textured solar cells (SCs). The model accounts for all recombination mechanisms, including nonradiative exciton recombination and recombination in the space-charge region (SCR). To compare the theoretical results with an experiment, we proposed empirical formula for the external quantum efficiency (EQE), which describes its experimental spectral dependencies near the absorption edge. The proposed approach allows modeling short-circuit current and photoconversion efficiency in the textured crystalline silicon solar cells. The theoretical results, compared to the experimental measurements, were used to optimize the key parameters of the SCs, such as the base thickness, doping level and others.**

Keywords— silicon, solar cell, texture, efficiency

I. Introduction

To reduce the cost of solar cells (SCs) while maximizing their photoconversion efficiency η, surface texturing techniques are used to reduce the optical reflection losses and maximize the light absorbed. Therefore, surface texturing of silicon photovoltaics systems is drawing much attention currently [1,2]. Recent record-breaking efficiency of 26.6% for Si solar cells have been achieved on such textured SCs ([3-5]), while the theoretical limit of the efficiency for Si SCs is about 29%. Therefore, to advance even more in improvement of the SCs efficiency the available optimisation approaches should be further developed and applied. In order to model and optimize textured high-efficiency silicon SCs we first measured and analyzed the experimental dependencies of the external quantum efficiency (EQE). Next, the calculated dependencies of the short-circuit current and the photoconversion efficiency under AM1.5 conditions on the base thickness d and its doping level are derived, and used to optimize the characteristics of textured silicon SCs. The texturing, an artificial roughening of the surface, reduces its reflection by increasing the chances of reflected light bouncing back onto the semiconductor surface, rather than out of it to the surrounding. The commonly accepted model for the textured surface from the reflection reduction point of view is a completely randomized Lambert surface [6]. However, the theoretical approach presented here is applicable to an arbitrary textured SCs surface.

It is established that the experimental spectral dependencies of the external quantum efficiency $EQE(\lambda)$ in textured silicon SCs near the absorption edge is described by an empirical formula $EQE(\lambda)=[1+b/(4n_r(\lambda)^2\cdot\alpha(\lambda)d)]^{-1}$, where $\alpha(\lambda)$ is the light absorption coefficient, d is the base thickness, n_r is the refractive index, and b is a non-dimensional coefficient, which characterizes the texturing quality. It is usually greater than 1, when b=1 the established empirical formula transforms into the well-known Yablonovitch formula [7]. Physical meaning of the parameter b is the ratio of the photon path length in the case of a perfectly randomized surface, considered in [6], to the photon path length in a particular sample with nonrandomized surface. This formula allows modelling and optimization the photo-conversion efficiency of the SC in terms of base thickness d.

This self-consistent approach for textured Si solar cells efficiency η of has been validated experimentally. Dark and light I–V characteristics as well as light intensity dependence of the open-circuit voltage were measured for a number of highly efficient silicon p-n junction SCs with the photoconversion efficiency $\eta \geqslant 20\%$. The spectral dependencies of $EQE(\lambda)$ under AM1.5 conditions were also investigated experimentally.

For the textured silicon SCs considered, the experimental dependencies of $EQE(\lambda)$ were analyzed. It is shown that close to the absorption edge $EQE(\lambda)$ behavior can be accurately described by the above empirical formula with the parameter b, ranging from 1.6 to 4. Using the experimental values $EQE(\lambda)$ and the proposed formula, we calculated the dependence of the short-circuit current density J_{SC} on the base thickness d for the textured SCs.

In the calculations and comparison of the theory with the experiment, in addition to the radiative and Auger recombinations we also considered nonradiative exciton recombination by the Auger mechanism via a deep recombination center [8] and recombination in the space charge region (SCR) [9].

II. Effective Recombination Time in Silicon

The minority carrier lifetime τ is one of the most important parameters for the characterization of semiconductor, used in SCs [10]. The total effective recombination time τ_{eff}, which includes all recombination mechanisms, can be written as:

$$\tau_{eff}(n) = \left[\frac{1}{\tau_{SRH}(n)} + \frac{1}{\tau_{nr}(n)} + \frac{S_{0S}}{d}\left(1 + \frac{\Delta n}{n_0}\right) + \frac{1}{\tau_r(n)} + \frac{1}{\tau_{Auger}(n)} + \frac{S_{SC}(n)}{d}\right]^{-1}, \quad (1)$$

where $n = n_0 + \Delta n$ is the total concentration of the majority carries (electrons, for definiteness) with the equilibrium concentration n_0, and the excess concentration of the electron-hole pairs (EHPs) Δn, $S_{0S} = S_{00} + S_{0d}$ is the total surface recombination velocity at the front and back surfaces of the solar cell in the low-injection regime, $\tau_{nr}(n) = \tau_{SRH} \cdot (n_x/n)$ is the nonradiative exciton recombination time [11], $\tau_r(n)$ is the radiative recombination time [12], and $\tau_{Auger}(n)$ is the Auger interband recombination time [13].

The Shockley–Read–Hall (SRH) recombination time τ_{SRH} for *n*-type Si can be written as:

$$\tau_{SRH}(n) \cong \frac{\tau_{p0}(n_0+\Delta n+n_1)+\tau_{n0}(p_1+\Delta n)}{(n_0+\Delta n)}, \quad (2)$$

where $\tau_{p0} = \left(C_p N_t\right)^{-1} s$ and $\tau_{n0} = (C_n N_t)^{-1} s$, with the hole (electron) capture coefficient C_p (C_n) by the recombination centers with concentration N_t, while n_1 and p_1 denote the electron and hole densities, respectively, when the Fermi level coincides with the trap level, the so-called Shockley-Reed factors for electrons and holes.

Note that the Shockley-Reed-Hall lifetime τ_{SRH} depends on the recombination center location inside the gap and the capture coefficient for electrons and holes. With increasing doping level and excitation level the lifetime changes in the range between two values, it can increase, decrease or practically remain constant. In the following we consider that the τ_{SRH} value is constant in the standard range of the doping levels and excitation (for the EHP excess concentration in the range from 10^{14} to 10^{16} cm^{-3}).

The expression for the radiative recombination lifetime can be written as [12]:

$$\tau_{rad}^{-1} = B\ (1 - P_{PR})\ (n_0 + \Delta n)\,, \quad (3)$$

where B is the radiative recombination parameter in silicon, and P_{PR} is the probability of photon reabsorption. Following [12], the expression for B is:

$$B = \int_0^\infty dE\ B(E), \text{ with } B(E) = \left(\frac{n_r(E)\ \alpha(E)\ E}{\pi\ c\ \hbar^{\frac{3}{2}}\ n_i}\right)^2 e^{-\frac{E}{k_B T}}. \quad (4)$$

Here $n_r(E)$ is the refractive index, and $\alpha(E)$ is the photon energy dependent absorption coefficient, $E = hc/\lambda$.

The probability of photon reabsorption can be defined as:

$$P_{PR} = B^{-1} \int_0^\infty dE\ A_{bb}(E)\ B(E)\,, \quad (5)$$

with the absorbance $A_{bb}(E)$ equals to

$$A_{bb}(E) = \frac{\alpha}{\alpha + b/4n_r^2 d}\,. \quad (6)$$

Expression (6) differs from that one from [7] in that it introduces a coefficient b greater than 1. As for the interband recombination lifetime $\tau_{Auger}(n)$, the empirical expression given in [13] is used.

The expression for the recombination rate in SCR S_{nr} is usually derived under the assumption that it occurs via a deep level, close to the middle of the band gap, and for the case of silicon it was presented and analyzed in [14], [15]. This was done in the model, when the discrete bulk deep level with the energy E_t is close to the middle of the band gap, with the concentration N_t^* and the capture cross sections of electron and hole σ_n and σ_p.

We used the following expression to calculate the recombination rate S_{nr} in the SCR (see [16], [17]):

$$S_{nr}(\Delta n) = \int_0^W \frac{(n_0+\Delta n)dx}{\left[\left((n_0+\Delta n)e^{y(x)} + n_i(T)\exp\left(\frac{E_t}{kT}\right)\right) + b_r\left((p_0+\Delta n)e^{-y(x)} + n_i(T)\exp\left(-\frac{E_t}{kT}\right)\right)\cdot\tau_R(x)\right]}\,. \quad (7)$$

Here $b_r = C_p/C_n$, $C_n = V_{nT}\sigma_n$, $C_p = V_{pT}\sigma_p$, with the average thermal velocities of electrons and holes V_{nT} and V_{pT}, $\tau_R(x) = (C_p N_t^*(x))^{-1}$ is the EHP lifetime in the SCR, N_t^* is the deep level concentration in the SCR, p_0 is the equilibrium bulk hole concentration, $y(x)$ is the dimensionless electrostatic potential in the SCR, E_t is the energy of the deep level in the silicon SCR, calculated from the middle of the gap, $n_i(T)$ is the concentration of intrinsic charge carriers, with the thickness of the SCR w.

To find the nonequilibrium dimensionless potential $y(x)$, we solve the second order integral Poisson equation in the following form:

$$x = \int_{y_0}^{y} \frac{L_D}{\left[\left(1+\frac{\Delta n}{n_0}\right)(e^{y_1}-1) - y_1 + \frac{\Delta n}{n_0}(e^{-y_1}-1)\right]^{0.5}} dy_1, \quad (8)$$

where $L_D = (\varepsilon_0 \varepsilon_{Si} kT/2q^2 n_0)^{1/2}$ is the Debye length, and q is the elementary charge.

The nonequilibrium dimensionless potential y_0 at x=0 can be found by solving the electroneutrality equation [14] in the form:

$$N = \pm\left(\frac{2kT\varepsilon_0\varepsilon_{Si}}{q^2}\right)^{1/2} [(n_0 + \Delta n)(e^{y_0} - 1) - n_0 y_0 + \Delta n(e^{-y_0} - 1)]^{1/2}, \quad (9)$$

where qN is the acceptors surface charge density in the *p-n* junction or unisotype heterojunction.

From Eq. (8) we obtain the following expression for the SCR thickness w:

$$w = \int_{y_0}^{y_w} \frac{L_D}{\left[\left(1+\frac{\Delta n}{n_0}\right)(e^{y}-1)-y+\frac{\Delta n}{n_0}(e^{-y}-1)\right]^{0.5}} dy, \quad (10)$$

where y_w is the nonequilibrium dimensionless potential at the boundary between the SCR and the quasi-neutral bulk.

Using the expressions (7) - (10), the S_{nr} dependence on the electron-hole pairs excess density Δn can be calculated.

Let's analyze the case when the lifetime in the SCR τ_R is small compared to the bulk lifetime, and τ_R is constant inside the space charge region d_0, in which the nonequilibrium dimensionless potential modulus is less than one. It is always less than the SCR width at the equilibrium *w* and much smaller than the base width *d*. If Δn is small enough ($\Delta n \ll n_0$), we obtain from (7) the recombination rate S_{sc} in the SCR. For the limit of large Δn ($\Delta n \gg n_0$) we can define the recombination rate d_0/τ_R, in the layer with a small lifetime τ_R. This occurs when the absolute value of the nonequilibrium dimensionless potential at the boundary of *n* and p^+layer is less than one, that is the bands are almost completely flattened. In the intermediate cases, we obtain from (7) a sum of the recombination rates in the SCR S_{SC} and $(d_0 - w(\Delta n))/\tau_R$, where $w(\Delta n)$ is the SCR thickness for a given Δn.

In the case when the lifetime in the SCR equals to that one of the bulk, this will not be the case. Since $w(\Delta n = 0) << d$, the addition to the bulk recombination rate due to the bands flattening $w(\Delta n < n_0)/\tau_b$, (τ_b is the bulk lifetime) will be very small compared to the bulk recombination rate and can always be neglected.

What happens if the typical silicon SCs parameters are used in the calculations? In the approximation of a constant SCR lifetime τ_r, the calculated slope of $S_{sc}(\Delta n)$ is higher than the experimental one, and agreement between the theory and experiment is not achieved when $\Delta n << n_0$ small lifetime values, no matter what the base thickness is. A much better agreement between the experiment and the theory can be achieved assuming the Gaussian distribution of the inverse life time in the SCR:

$$\tau_R{}^{-1}(x) = \tau_m^{-1}\, exp\left(\frac{-(x-x_m)^2}{2\sigma^2}\right), \quad (11)$$

where τ_m is the life time at the point of maximum, x_m is a position of the maximum, and σ is the dispersion.

In this case $S_{sc}(\Delta n) \equiv S_{nr}(\Delta n)$, by reducing the half-width of the gaussian a faster decrease of $S_{sc}(\Delta n)$ can be achieved. Sufficiently large values of $S_{sc}(\Delta n)$ for small Δn can be achieved by reducing the lifetime τ_m.

Note that for the SCs with rear contact metallization, recombination in the SCR does not occur over the entire SC area A_{SC}. It happens only in the places where inversion band bending occurs, that is in the area, doped with boron, with its surface A_B less than A_{SC}. Therefore, for this case in the expression (1) it is necessary to write $S_{SC}\cdot(A_B/A_{SC})$ instead of S_{SC}.

III. Modeling photoconversion efficiency at AM1.5

The light *I-V* characteristics for the rear contact solar cells (RCSCs) under consideration (they are also called interdigitated back contact solar cells (IBCSCs)) were calculated using the expressions from [9, 11, 12]:

$$I(V) = I_L - \frac{qA_{SC}d\ \Delta n}{\tau_{eff}(\Delta n)} - \frac{V+IR_S}{R_{sh}} \quad (12)$$

$$I_r(V) = qA_{SC}\left(\frac{d}{\tau_{eff}^b} + S_{00s}\left(1+\frac{\Delta n}{n_0}\right) + \frac{A_B}{A_{SC}}S_{sc}\right)\Delta n(V), \quad (13)$$

$$\tau_{eff}^b(n) = \left[\frac{1}{\tau_{SRH}} + \frac{1}{\tau_r(n)} + \frac{1}{\tau_{nr}(n)} + \frac{1}{\tau_{Auger}(n)}\right]^{-1}, \quad (14)$$

$$\Delta n(V) = -\frac{n_0}{2} + \sqrt{\frac{n_0^2}{4} + n_{i0}(T)^2 e^{\Delta E_g/kT}\left(exp\frac{q(V-IR_S)}{kT} - 1\right)}, \quad (15)$$

where $I(V)$ is the full current, I_L is the photogeneration current, $I_r(V)$ is recombination (dark) current, V is applied voltage, $\tau_{eff}^b(n)$ is effective bulk lifetime, R_s and R_{SH} are series and shunt resistances, n_{i0} is the intrinsic concentration at low injection [18], and $\Delta E_g\ (n_0, \Delta n)$ is the magnitude of bandgap narrowing in Si [13].

The expression for the dark current according to (12) has the form:

$$I_D(V) = \frac{qA_{SC}d\ \Delta n}{\tau_{eff}(\Delta n)} + \frac{V-I_D R_S}{R_{sh}}. \quad (16)$$

The photogeneration current I_L dependence on the open circuit voltage V_{OC} can be found from (12) by putting $I = 0$:

$$I_L = \frac{A_{SC}qd}{\tau_{eff}(\Delta n_{OC})}\Delta n_{OC} + \frac{V_{OC}}{R_{sh}}, \quad (17)$$

with

$$\Delta n_{OC} = -\frac{n_0}{2} + \sqrt{\frac{n_0^2}{4} + n_{i0}^2 e^{\Delta Eg/kT}(e^{qV_{OC}/kT} - 1)}. \quad (18)$$

If we compare the expressions for Δn and Δn_{OC}, as well as the dark current (17) and photogeneration current (18), one sees that they coincide with each other, if we replace V by V_{OC} and I_D by I_L and also put R_S in (15) to zero.

This means that the solutions $I_D(V, R_{sh}, R_s)$ and $I_L(V_{OC}, R_{sh})$ are identical if $R_S = 0$. And $V_{OC}(\Delta n_{OC})$ can be found from (18):

$$V_{OC} = \frac{kT}{q} ln\left(\frac{(\Delta n_{OC}+n_0)\cdot\Delta n_{OC}}{n_{i0}(T)^2 e^{\Delta Eg/kT}} + 1\right). \quad (19)$$

Multiplying current *I(V)* on the applied voltage *V*, we get the power $P(V)$, and maximizing this from dP/dV=0 condition we find the voltage V_M at the point of maximum power. Substituting V_M in equation (12), we obtain the current at the maximum power point I_M. This allows calculating photoconversion efficiency η and the *I–V* fill-factor *FF* in the usual way. Note that in the approximation used, the short-circuit current I_{SC} value is a parameter.

On the other hand, the short-circuit current in the textured silicon SCs can be calculated if the external quantum efficiency of the photocurrent $EQE(\lambda)$ is known. As it was shown in [19],

for a number of high efficiency textured silicon SCs with *p-n* junctions and *HIT* elements, the external quantum yield in the long-wavelength region is described by the following empirical formula:

$$EQE(\lambda)=[1+b/(4n_r(\lambda)^2\cdot\alpha(\lambda)d)]^{-1} \quad (20)$$

where b is a numerical coefficient larger than one. More details will be given later in Fig. 7, which shows experimental dependence of $EQE(\lambda)$ for the SCs considered and their approximation by expression (20). The value b=4 leads to a good agreement of the experimental and calculated dependencies in the long-wavelength region. As can be seen from the figure, for the SCs considered the expression (20) describes accurately the experimental $EQE(\lambda)$ dependencies in the range from 1200 to 800 nm. Therefore, for the above IBCSC the short-circuit current density J_{SC} at AM 1.5 can be calculated by the formula

$$J_{SC}(d,b) = q\left[\int_{\lambda_0}^{800} I_{AM1,5}(\lambda)EQE(\lambda)d\lambda + f\int_{800}^{\lambda_m} I_{AM1,5}(\lambda)EQE(\lambda,b)d\lambda\right], \quad (21)$$

where λ_0 = 300 nm, λ_m = 1200 nm, $I_{AM1.5}(\lambda)$ is the spectral density of the photon flux at AM 1.5, $EQE(\lambda,b)$ is determined by expression (20), and the coefficient $f \le 1$. The f value is chosen in such a manner that at λ = 800 nm the values $EQE(\lambda,b)$ and $IQE(\lambda,b)$ coincide. In this way J_{SC} dependence on the base thickness d can be found, which allows to optimize the SCs on the base thickness.

IV. The Results and Analysis

To validate the above theoretical approach developed and its application, we characterised experimentally the commercial textured silicon *p-n* junction SCs with a photoconversion efficiency η above 21%, which are manufactured by Sun Power. The SCs with rear metallization, have a photoactive area of 154.7 cm^2 and the base thickness d = 165 μm. Fig. 1 shows the dark *I–V* characteristic of one of the solar cells studied.

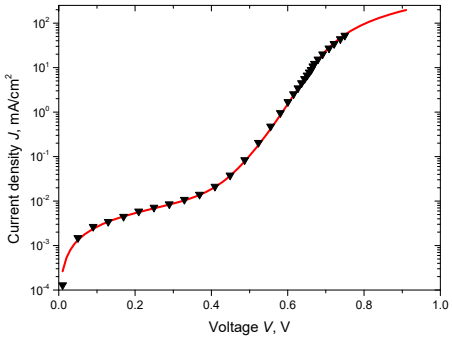

Fig. 1. Dark *I-V* characteristic of the Sun Power solar cell. Triangles are the experimental values; the solid line is from our theory.

To theoretically model dark *I–V* characteristics, it is necessary to find the recombination parameters, in particular τ_R and b_r, that determine the recombination rate in the SCR. When modeling the SCR recombination, we consider its Gaussian-like dependence as given by (11).

The above theory has been compared to the experimental $J_r(V)$ dependence that we measured. The following parameters: n_0= 9·10^{14} cm^{-3}, d = 165 μm, τ_m = 1.3 · 10^{-5} s, x_m= 180 nm, σ = 50 nm, and b_r= 0.1 were obtained from the fit: the total rate of the surface recombination at a low excitation level S_{0s} is 5 cm/s. We assumed in the simulation that τ_{SRH} = 10 ms, which is well-matched to [20].

Fig. 2 shows the theoretical $S_{sc}(\Delta n)$ dependence, plotted using the same parameters, used in Fig. 1:

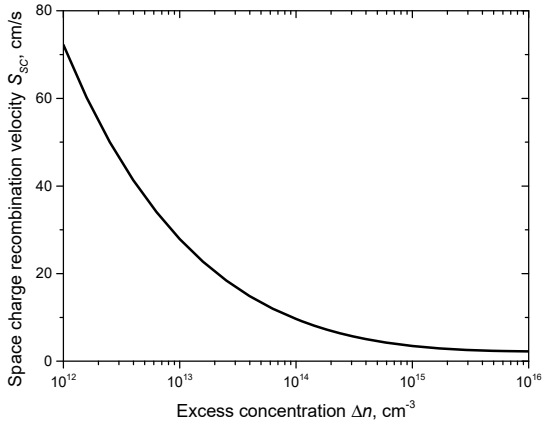

Fig. 2. Theoretical dependence of the recombination velocity in SCR on the excess concentration, $S_{SC}(\Delta n)$.

Fig. 3 shows the light *I–V* characteristic, measured at AM1.5, for the Sun Power SC with the open circuit voltage V_{OC}= 0.692 V, and the short-circuit current density J_{SC} = 40.04 mA/cm^2. Experimental and calculated light *I–V* characteristics agree well when using the same components of the effective life time as the dark *I–V* characteristics.

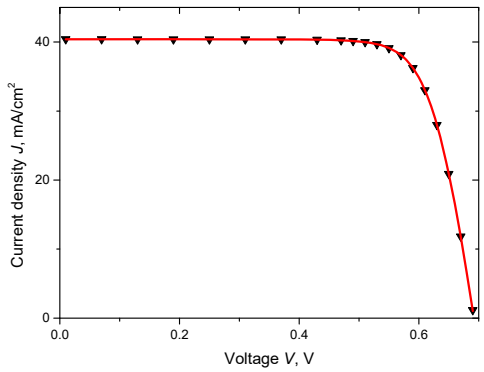

Fig. 3. Measured and calculated light *I–V* characteristics. Triangles are the experimental values; the solid line is from the theory.

Next, Fig. 4 demonstrates the experimental dependence of the photocurrent density J_L on the open circuit voltage V_{OC} for SC at temperature of 25°C. In contrast to similar dependencies, reported in the literature (see, for example, [3],

[4]), these dependencies are both measured and calculated in a much wider range of J_L, including, in particular, the region of low photocurrent density J_L. Estimates show that at J_L <10^{-5}A/cm^2 the inequality $V_{OC}/R_{sh} > J_L$ holds.

In the case when $J_L = 4\cdot10^{-2}$A/cm^2, compared to that J_L the V_{OC}/R_{sh} value is two and a half orders of magnitude less and can be neglected in Eq. (17).

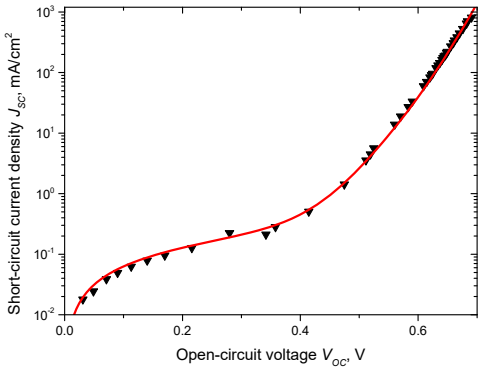

Fig. 4. Short-circuit current density J_{CS} dependence on the open-circuit voltage V_{OC}. Triangles are the experimental results, while solid line is the theory.

The theoretical $J_{SC}(V_{OC})$ dependence can be found from a joint solution of Eqs. (17) and (18) using the same parameters as for calculation of the dark *I–V* characteristic. As can be seen from Fig. 4, there is a good agreement between the experiment and the theory. A comparison between Figs. 1 and 4 also shows that when V and V_{OC} are less than 0.68 V, the solutions $J_D(V)$ and $J_L(V_{OC})$ coincide. This is consistent with the above analysis.

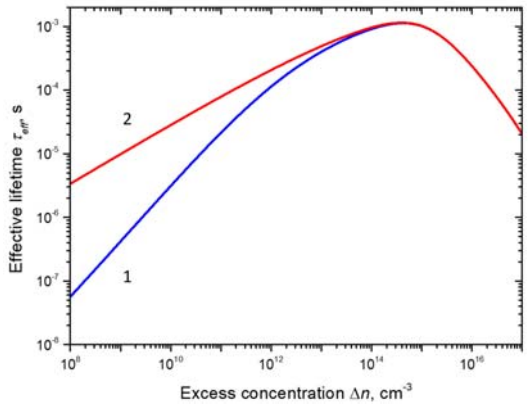

Fig. 5. Theoretical $\tau_{eff}(\Delta n)$ dependencies. Upper curve 1 (blue line) is calculated using Eq. (22), while the curve 2 above (red line) is from Eq. (23).

We plot the $\tau_{eff}(\Delta n_{OC})$ dependence in Fig. 5 using the expressions (22) and (23):

$$\tau_{eff1} = \left(\frac{J_L+\frac{V_{OC}}{R_{sh}}}{\Delta n_{OC} q d}\right)^{-1}, \qquad (22)$$

$$\tau_{eff2} = \left[\frac{1}{\tau_{SRH}} + \frac{1}{\tau_r(\Delta n_{OC})} + \frac{1}{\tau_{nr}(\Delta n_{OC})} + \frac{1}{\tau_{Auger}(\Delta n_{OC})} + \frac{S_{00s}}{d}\left(1+\frac{\Delta n_{OC}}{n_0}\right) + \frac{A_B}{A_{SC}}\frac{S_{SC}}{d}\right]^{-1}. \qquad (23)$$

The two graphs 1 and 2 in Fig. 5 differ on whether the short-circuit current density component $\frac{V_{OC}}{R_{sh}}$ is included (curve 1) or neglected (curve 2). As can be seen from Fig. 5, at the right of the τ_{eff} maximum both curves depend on Δn_{OC} identically, while at the left of the maximum they deviate. Therefore, the $\frac{V_{OC}}{R_{sh}}$ component has to be included into consideration, as it is done for the accurate curve 1. However, further modeling in order to find the open circuit voltage V_{OC} and photoconversion efficiency η using the expression (19) for V_{OC} and η, shows that both dependencies provide the correct results. In particular, at S_{00s} = 5 cm/s the experimental and theoretical V_{OC} values coincide, while the experimental and calculated photoconversion efficiencies are also the same, η= 21.5% (R_s = 1.1 Ohm·cm^2 is chosen). As well, in this case the experimental and calculated *I–V* filling factors, equal to 87.7%, coincide.

Fig. 6 shows the calculated efficiency η dependence on the base doping level n_0. As can be seen from the figure, the maximum of $\eta(n_0)$ = 21.69% is reached at n_0= 5.5 · 10^{15} cm^{-3}, this differs from the experimental value by less than one percent.

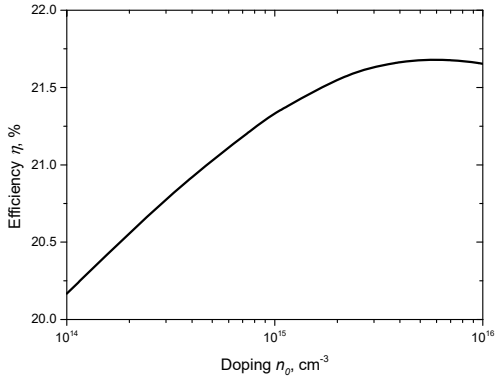

Fig. 6. Theoretical dependence of the photoconversion efficiency η on the base doping level n_0. Its maximum of 21.69% is achieved at at n_0= 5.5 · 10^{15} cm^{-3}

Fig. 7 shows the experimental external quantum efficiency $EQE(\lambda)$, which we measured, for the SC sample studied. Using the expression (18), the coefficient *b* from the phenomenological formula (20) for $EQE(\lambda)$ in the long-wavelength range can be found and it equals to 4. Using b = 4, as well as the expression (19) for the base thickness d dependent short-circuit current, we can calculate the base thickness dependent photoconversion efficiency, which is shown in Fig. 8. As can be seen from the figure, the maximum η = 21.72% is reached at d = 750 μm, which is one percent above the experimental value.

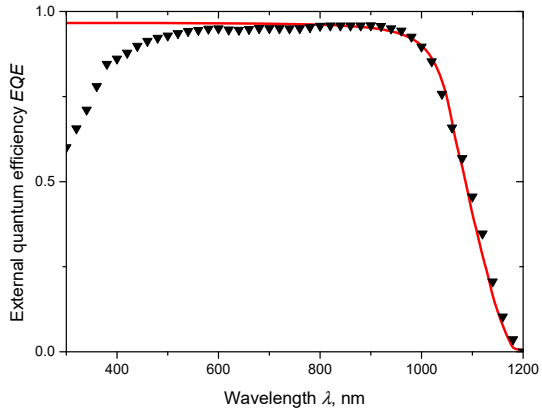

Fig. 7. Experimental (triangles) and theoretical (calculated by formula (20) red line) dependencies of $EQE(\lambda)$.

a.

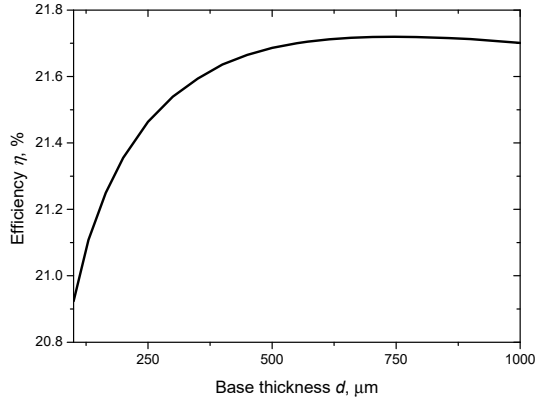

Fig. 8. The photoconversion efficiency η dependence on the base thickness d. The efficiency maximum $\eta = 21.72\%$ is achieved at $d = 750$ μm.

V. Conclusions

We proposed a comprehensive formalism to model and optimize the high efficiency textured silicon-based solar cells. It is demonstrated that the contribution of nonradiative exciton recombination, as a rule, exceeds the radiative recombination contribution and substantially affects the photoconversion efficiency, stronger than the gap narrowing effect.

We investigated experimentally the open-circuit voltage V_{OC} dependent photocurrent density $J_{SC}(V_{OC})$ in a wide range of the photocurrent density, which allows extracting correct dependence of the lifetime $\tau_{eff}(\Delta n)$ on the excess concentration Δn. As can be seen from the dependencies, at $\Delta n < 4 \cdot 10^{14}$ cm^{-3} the value of τ_{eff} decreases with decreasing Δn, which indicates a significant effect of recombination in the SCR in the area with excess concentrations of electron-hole pairs. This is also evidenced by the dark I–V characteristics of the SCs, studied in the work.

The proposed approach allows to correctly model the short-circuit current and the efficiency of photoconversion in the high efficiency textured silicon solar cells. The formalism allows to self-consistently calculate such key SCs parameters as the short-circuit current density J_{SC}, open-circuit voltage V_{OC} and photoconversion efficiency η. Such calculations have been carried out for several SCs types achieving very good agreements of calculated characteristics with experimental ones. This allows also to optimize the SCs base thickness and the doping level.

It is also shown that the recombination in SCR decreases the effective recombination time $\tau_{eff}(\Delta n)$ in the region of small values of Δn.

As it can be concluded from our analysis, the standard experimentally measured SCs characteristics are usually not sufficient to comprehensively model and optimize the textured silicon SCs. To carry out such modeling, the experimental dependence $\tau_{eff}(\Delta n)$, measured on the assembled SCs, or the experimental dark I–V characteristics are also required.

Acknowledgment

This work was partially supported (V. Kostylyov and V. Vlasiuk) by National Research Foundation of Ukraine by the state budget finance (project 2020.02/0036 “Development of physical base of both acoustically controlled modification and machine learning–oriented characterization for silicon solar cells”).

References

[1] J. Liu, Y. Yao, S. Xiao, and X. Gu, J. Phys. D, vol. 51, pp. 123001-123013, February 2018.

[2] A. Augusto, J. Karas, P. Balaji, S. G. Bowden, and R. R. King, J. Mater. Chem. A, vol. 8, pp. 16599-16608, October 2020.

[3] K. Yoshikawa, W. Yoshida, T. Irie, H. Kawasaki, K. Konishi, H. Ishibashi, T. Asatani, D. Adachi, M. Kanematsu, H. Uzu, et al, Solar Energy Mater. Solar Cells, vol. 173, pp. 37-42, June 2017.

[4] K. Yoshikawa, H. Kawasaki, W. Yoshida, T. Irie, K. Konishi, K. Nakano, T. Uto, D. Adachi, M. Kanematsu, H. Uzu, et al, Nature Energy, vol. 2, pp. 17032-17041, May 2017.

[5] M. Green, E. Dunlop, J. Hohl-Ebinger, M. Yoshita, N. Kopidakis, and X. Hao, Prog Photovoltaics Res Appl, vol. 29, pp. 3-15, January 2021.

[6] M. A. Green, Prog. Photovolt: Res. Appl., vol. 10, pp. 235-241, February 2002.

[7] T. Tiedje, E. Yablonovitch, G. D. Cody, and B. G. Brooks, IEEE Trans. Electron Devices, vol. 31, pp. 711-716, May 1984.

[8] A. V. Sachenko, Y. V. Kryuchenko, V. P. Kostylyov, A. V. Bobyl, E. I. Terukov, S. N. Abolmasov, A. S. Abramov, D. A. Andronikov, M. Z. Shvarts, I. O. Sokolovskyi, et al, J. Appl. Phys., vol. 119, pp. 225702-225711, June 2016.

[9] A. Sachenko, V. Kostylyov, V. Vlasiuk, I. Sokolovskyi, and M. Evstigneev, 47th IEEE Photovoltaic Specialists Conference (PVSC), pp. 0719-0725, 2020.

[10] T. Niewelt, A. Richter, T. C. Kho, N. E. Grant, R. S. Bonilla, B. Steinhauser, J. -. Polzin, F. Feldmann, M. Hermle, J. D. Murphy, et al, Solar Energy Mater. Solar Cells, vol. 185, pp. 252-259, June 2018.

[11] A. V. Sachenko, V. P. Kostylyov, V. M. Vlasiuk, I. O. Sokolovskyi, and M. Evstigneev, J Lumin., vol. 183, pp. 299-303, November 2016.

[12] A. Sachenko, V. Kostylyov, I. Sokolovskyi, and M. Evstigneev, IEEE Journal of Photovoltaics, vol. 10, pp. 63-69, Janury 2020.

[13] A. Richter, S. W. Glunz, F. Werner, J. Schmidt, and A. Cuevas, Phys.Rev.B, vol. 86, pp. 165202-165216, October 2012.

[14] A. P. Gorban, V. P. Kostylyov, A. V. Sachenko, A. A. Serba, and I. O. Sokolovsky, Ukr. J. Phys., vol. 51, pp. 598-604, June 2006.

[15] A. V. Sachenko, V. P. Kostylyov, I. O. Sokolovskyi, A. V. Bobyl', V. N. Verbitskii, E. I. Terukov, and M. Z. Shvarts, Technical Physics Letters, vol. 43, pp. 152-155, February 2017.

[16] C. Sah, R. N. Noyce, and W. Shockley, Proceedings of the IRE, vol. 45, pp. 1228-1243, September 1957.

[17] A. V. Sachenko, V. P. Kostylyov, V. M. Vlasiuk, R. M. Korkishko, I. O. Sokolovs'kyi, and V. V. Chernenko, Ukr. J. Phys., vol. 61, 917-925, October 2019.

[18] A. B. Sproul and M. A. Green, J. Appl. Phys., vol.73, pp. 1214-1225, March 1993.

[19] A. V. Sachenko, V. P. Kostylyov, A. V. Bobyl, V. N. Vlasyuk, I. O. Sokolovskyi, G. A. Konoplev, E. I. Terukov, M. Z. Shvarts, and M. Evstigneev, Technical Physics Letters, vol. 44, pp. 873-876, October 2018.

[20] D. D. Smith, G. Reich, M. Baldrias, M. Reich, N. Boitnott, and G. Bunea, Proceedings IEEE PVSC 43, pp. 3351–3355, June 2016.